Control of bacterial biofilm growth on surfaces by nanostructural mechanics and geometry



2011 Nanotechnology 22 494007

(http://iopscience.iop.org/0957-4484/22/49/494007)

Nanotechnology **22** (2011) 494007 (8pp) doi:10.1088/0957-4484/22/49/494007

# Control of bacterial biofilm growth on surfaces by nanostructural mechanics and geometry

**A K Epstein**[1,2], **A I Hochbaum**[1,3], **Philseok Kim**[1,2] **and J Aizenberg**[1,2,3]

[1] School of Engineering and Applied Sciences, Harvard University, 29 Oxford Street, Cambridge, MA 02138, USA
[2] Wyss Institute for Biologically Inspired Engineering, 3 Blackfan Circle, Boston, MA 02115, USA
[3] Department of Chemistry and Chemical Biology, Harvard University, 12 Oxford Street, Cambridge, MA 02138, USA

E-mail: jaiz@seas.harvard.edu

Received 28 June 2011, in final form 22 October 2011
Published 21 November 2011
Online at stacks.iop.org/Nano/22/494007

**Abstract**
Surface-associated communities of bacteria, called biofilms, pervade natural and anthropogenic environments. Mature biofilms are resistant to a wide range of antimicrobial treatments and therefore pose persistent pathogenic threats. The use of surface chemistry to inhibit biofilm growth has been found to only transiently affect initial attachment. In this work, we investigate the tunable effects of physical surface properties, including high-aspect-ratio (HAR) surface nanostructure arrays recently reported to induce long-range spontaneous spatial patterning of bacteria on the surface. The functional parameters and length scale regimes that control such artificial patterning for the rod-shaped pathogenic species *Pseudomonas aeruginosa* are elucidated through a combinatorial approach. We further report a crossover regime of biofilm growth on a HAR nanostructured surface versus the nanostructure effective stiffness. When the 'softness' of the hair-like nanoarray is increased beyond a threshold value, biofilm growth is inhibited as compared to a flat control surface. This result is consistent with the mechanoselective adhesion of bacteria to surfaces. Therefore by combining nanoarray-induced bacterial patterning and modulating the effective stiffness of the nanoarray—thus mimicking an extremely compliant flat surface—bacterial mechanoselective adhesion can be exploited to control and inhibit biofilm growth.

S Online supplementary data available from stacks.iop.org/Nano/22/494007/mmedia

(Some figures may appear in colour only in the online journal)

## 1. Introduction

Bacteria often form structured, multicellular communities, called biofilms, on surfaces in natural and anthropogenic environments [1]. Biofilms contaminate a wide variety of infrastructures, such as plumbing, oil refineries, paper mills, heat exchangers, medical implants and building HVAC systems [2]. Marine fouling, which is precipitated by the accumulation of bacterial biofilm on ship hulls followed by progressively larger marine organisms, increases the fuel expenditure of seafaring vessels by up to 40% [3]. And in medical settings, biofilms are the cause of persistent infections, triggering immune response, release of harmful toxins and even obstructing indwelling catheters. As a result, hospital-acquired (or nosocomial) infections affect about 10% of patients in the United States, accounting for nearly 100 000 deaths annually. Moreover, biofilms have been estimated to cause 80% or more of all microbial infections in humans [4, 5].

Biofilms protect their constituent cells in various ways, which makes both clinical and industrial contamination difficult to treat. As self-organized communities, biofilms have evolved to feature differentiated cell phenotypes

 

performing complementary functions. The associated cooperative behavior of bacterial cells, mediated by cell–cell communications and other factors, enables an increased metabolic diversity and efficiency as well as an enhanced resistance to environmental stress, antimicrobial agents and the host's defenses [6, 7]. Biofilms organize into spatial patterns at the macroscopic and microscopic level. For example, some constituent cells are active in spreading the biofilm while others enter dormant states invulnerable to antimicrobials based on metabolic or reproductive pathways [8–11]. The macroscopic physical properties of biofilms are reported to also protect constituent cells, resisting conventional liquid and vapor phase treatments [12].

A wide range of bacterial-resistant surfaces have been proposed to inhibit biofilm growth *a priori*, but the typical strategies rely either on a release of biocidal compounds or on inhibiting adhesion. In the first case, traditional techniques involve the design of coatings that release agents such as antibiotics, quaternary ammonium salts and silver ions into the surrounding aqueous environment. Such agents have been incorporated into a variety of engineering polymers and other materials [13]. The latter approach has focused on the use of surface chemical functional groups that prevent protein adsorption as a means to inhibit bacterial adhesion. One of the most commonly studied such surface modifications is poly(ethylene glycol), or PEG [14, 15].

Both of these strategies, however, are transient. Materials that persistently resist bacteria are difficult to achieve by surface chemistry alone. Even if bacteria are unable to attach directly to a substrate, nonspecific adsorption of proteins and surfactants secreted by bacteria to the surface eventually masks the underlying chemical functionality [16–18]. Over a longer timescale, the reservoir of leaching antimicrobial compounds is normally finite and subject to depletion. Also, the emergence of antibiotic-and silver-resistant pathogenic strains, along with new restrictions on the use of biocide-releasing coatings in the marine environment, have necessitated the development of new strategies [19–21].

In contrast, the effects of topographical features on bacterial adhesion and biofilm formation are poorly understood. Nature provides some clues to preventing microbial colonization of surfaces by this alternative strategy. For example, ship hulls constantly amass layers of algae and crustaceans. Yet materials with topographical features mimicking the skin of sharks have shown increased resistance to marine biofouling at certain length scales [22]. Physical structures may provide a more persistent form of inhibitive interaction between bacteria and surfaces. Indeed, mammalian cells respond to surface topography and mechanics and their behavior can be manipulated using only spatial and mechanical cues [23–25]. Bacteria have also been reported to respond to mechanical cues. Surface attachment is an integral step in biofilm formation and impacts chemical signaling pathways between and within bacterial cells [26]. Substrate elastic modulus, for example, has been suggested to affect the density of surface colonization. Specifically, on flat surfaces in the Young's modulus range of 1–100 MPa, a positive correlation is reported between attachment density and surface modulus [27]. Topographical features can influence the arrangement and the resulting behavior of cells on surfaces and may affect biofilm development [28]. However, the roles of specific surface structures in modifying bacterial attachment and subsequent behavior—particularly the role of geometric parameters relative to the mechanical properties of the surface structures—remain unclear.

Here we present new findings on the interactions governing bacterial assembly on nanopost substrates. The attachment and biofilm accumulation behavior were studied by altering the symmetries, dimensions and pitch (center-to-center distance) of nanopost arrays using a combinatorial approach. Additionally, the attachment of bacteria to nanostructured substrates as a function of the effective stiffness was investigated and compared to the attachment to flat, unpatterned surfaces. Rather than rely on intrinsic material modulus, we exploit a derived effective stiffness, dependent on both the material and geometric properties of the surface, to direct bacterial adhesion and to affect biofilm growth.

## 2. Experimental details

### *2.1. Substrate fabrication*

Nanostructured substrates were fabricated with feature dimensions on the order of the size of bacterial cells. Arrays of high-aspect-ratio nanometer-scale polymer posts were generated in UV-curable epoxy (Epoxy Technology UVO-114) and polyurethanes (Norland Optical Adhesives (NOA) 61 and 65) using a fast polymer replication technique described previously [29]. Sets of replicas with varying dimensional parameters, including nanopost diameter, pitch and array symmetry, were molded using different microfabricated Si masters and geometric manipulations of polydimethylsiloxane (PDMS, Dow Corning Sylgard 184) molds.

Several experiments used a combinatorial substrate of posts in an array of square symmetry with a variation of the pitch of posts from one end of the substrate to the other. To make the rectangular symmetry post array with a pitch gradient, a replica was made from a uniaxially stretched PDMS mold of a square array pitch gradient pattern. The mold was stretched and the epoxy was cured on the stretched mold. The array consisted of posts having a diameter of about 300 nm and a height of about 2 $\mu$m.

Post substrates with orthogonal post pitch and diameter gradients were fabricated using the STEPS method described previously [30]. An epoxy (UVO-114) replica of a nanopost array, containing a pitch gradient from 4.0 down to 0.8 $\mu$m across the substrate, was sputter-coated with 50 nm of Au to make the surface electrically conductive. The gold-coated sample was then 80% submerged into an electrochemical cell with 0.1 M pyrrole monomer and 0.1 M sodium dodecylbenzenesulfonate aqueous solution as an electrolyte. Potentiostatic (0.55 V versus Ag/AgCl) electrodepositions of polypyrrole were employed with stepwise withdrawal of the sample in the direction perpendicular to the pitch gradient in four equal, discrete steps at $t$ = 15, 30, 45 and 60 min (figure 2(a)). Between time points the sample was

stationary with 30 min of equilibration and drying time. Since the withdrawal direction was perpendicular to the pitch gradient, an orthogonal gradient of nanostructure diameter corresponding to the PPy growth time was obtained.

Polymer replicas consisting of square post arrays were also fabricated from UVO-114, NOA 61 and NOA 65—to vary substrate stiffness—by curing under UV lamps at 130 mW $cm^{-2}$ (at 365 nm) for 20, 60 and 60 min, respectively. These arrays had dimensions of 2 $\mu$m pitch, 250 nm diameter and 8 $\mu$m tall posts with a projected area of 4 $cm^2$. Flat substrates of equal area were fabricated from the same polymers to serve as controls.

### *2.2. Measurement of Young's modulus*

The Young's moduli of the NOA 61 and NOA 65 polymers were determined by the four-point flexure method previously described [29], except that the flexure samples were fabricated, in triplicates, with the following dimensions: length = 40 mm, width = 5 mm, thickness = 1.5 mm and the mechanical measurements were performed on an Instron 5566 universal test system.

### *2.3. Bacterial preparation and growth*

*Pseudomonas aeruginosa* (strain PA14) was grown in Luria broth (LB) medium (EMD LB Broth Miller) overnight at 37 °C in loosely capped tubes on an orbital shaker to the stationary phase. This LB preculture was then seeded at 1% concentration in TB growth medium (BD Bacto Tryptone) on polymer substrates attached with carbon tape to the bottoms of six-well plates. Samples were immersed in 4 ml of inoculated medium and grown on the bench at room temperature for various time points.

### *2.4. Imaging and analysis*

For fluorescence imaging of attached bacterial cells, the growth culture was aspirated from each well, the submerged polymer samples were gently rinsed in the well with phosphate buffered saline (PBS) (1×) (Lonza Biowhittaker) and the adherent bacteria were fixed by 5% glutaraldehyde solution for at least 1 h. Following another PBS rinse, 0.01% Triton X100 in PBS (PBST) was used to permeabilize the bacteria membranes. Next the cells were stained with 0.5 $\mu$M SYTOX green nucleic acid stain (Invitrogen) in PBST for 30 min, after which they were rinsed in PBS for fluorescence imaging.

To analyze the ordering present in different fluorescence micrographs, fast Fourier transforms (FFT) were performed and contrast-optimized using ImageJ.

### *2.5. Bacterial quantification by sonication and colony forming units (CFU)*

The attached bacteria or biomass on various polymer samples was quantified using a multi-step process of cell removal, serial dilution and plating for viable cell counts. First, each polymer sample was individually placed into a 50 ml conical tube containing 15 ml of 3 mM D-tyrosine in PBS at pH 7.5 and incubated at room temperature for 30 min to promote biofilm disassembly. The samples were bath-sonicated for 10 min. 200 $\mu$l of each sonicated solution was pipetted into a 96-well plate and serially tenfold-diluted. 10 $\mu$l of each serial dilution of each sample were pipetted in parallel onto an LB agar plate, which was briefly tilted to spread the drops into parallel lines and was then incubated for 36–48 h at room temperature. Bacterial colony forming units (CFU), individual bacteria that reproduce into visible colonies, were counted on each plate and the CFU values were compared at corresponding dilution factors.

## 3. Results and discussion

### *3.1. Topographical effects on the alignment of bacteria*

The replication method used to fabricate the polymer high-aspect-ratio (HAR) nanopost substrates can be modified to create post arrays with a range of dimensions and symmetries from the same elastomeric molds [29]. Applying precise sets of deformations to the elastomeric molds while the replica material is cured in them allows nanopost cross sections to be proportionally elongated, nanoposts to be tilted away from the vertical axis and the array to be transformed from square to rectangular or rhombic. Additionally, substrate curvature or twist can be introduced. These substrate modifications are possible either through simultaneous mold deformations or through iterative mold deformation and replication steps.

*3.1.1. Directed cell alignment by topographical cues.* In particular, the fourfold symmetry of the square post array used in pitch gradient samples can be broken by uniaxial extension of the mold during the substrate curing step. In this manner, the square post array is transformed into a rectangular array, where the post pitch is expanded in one lattice direction and contracted in the orthogonal direction due to Poisson compression (figure 1(a)). Previous work demonstrated the spontaneous assembly of bacteria on periodic post arrays and suggested a model for bacterial patterning by surface contact area maximization [28]. With this principle in mind, we designed substrates to align bacterial adhesion on surfaces using only topographical cues.

Using uniaxial extension of a surface with square symmetry and a spatial post pitch gradient across the substrate during the curing step, we generated a rectangular post array with spatially varying pitch along both lattice parameters. *P. aeruginosa* was cultured on these anisotropic HAR nanopost arrays and their self-assembled patterns were observed by fluorescent microscopy (figure 1(b)). Consistent with previous results [28], the bacteria attach in different configurations depending on the pitch of the posts. At the small-pitch extreme (0.9 $\mu$m) the bacteria align themselves with the posts, oriented normal to the substrate, forming a rectangular array on the surface. As the post pitch increases the bacteria align themselves in the orthogonal directions of symmetry of the array by lying in the plane of the substrate.

The organizational characteristics of the bacterial patterns are more clearly seen in the Fourier transforms (FFT) of the

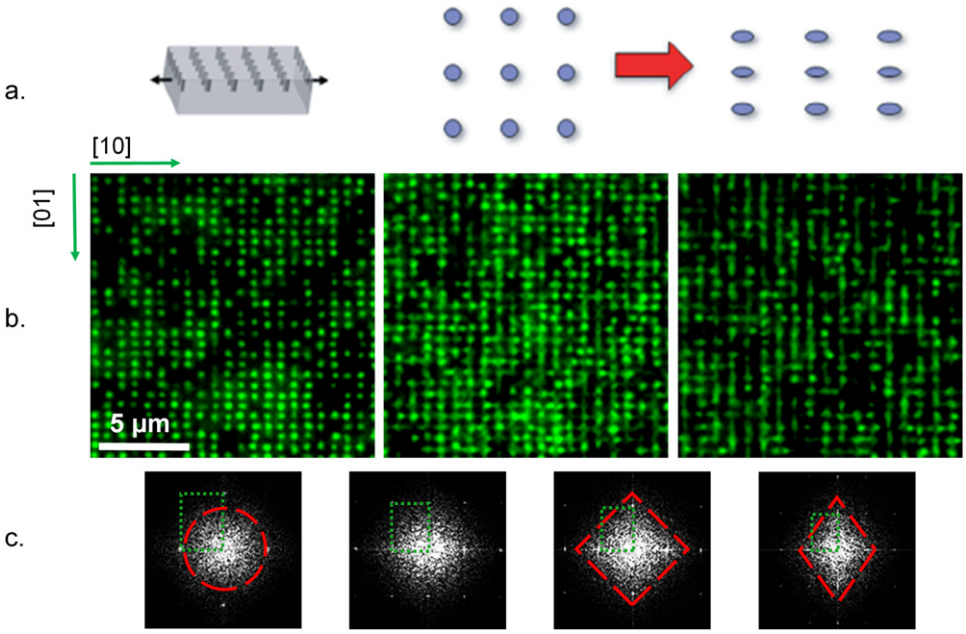


**Figure 1.** (a) Schematic of uniaxial elastomeric mold stretching and the resultant nanopost array transformation from square to rectangular symmetry. (b) Fluorescence images of *P. aeruginosa* bacteria following 18 h growth on nanopost substrates with rectangular symmetry and increasing pitch in both directions from the left image to the right one. The vertical [01] lines of bacteria in the rightmost image are consistent with surface contact area maximization as a driver for spontaneous attachment. (c) From left to right, Fourier transforms of rectangular high-aspect-ratio nanopost arrays show the induced directional patterning of bacteria by surface structure periodicity alone. The elongation of the central spot indicates that bacteria preferentially lie along the [01] direction.

fluorescence intensity images (figure 1(c)). The small points correspond to positional ordering peaks and the anisotropy of the diffuse central spot corresponds to the orientational ordering of the rod-like cells. The positional ordering peaks are spaced at larger distances along the [01] vertical direction (corresponding to smaller post spacing in real space) than in the [10] horizontal directions, indicating cellular registration with the rectangular post symmetry. Within the closely spaced posts, where the cells align normal to the substrate, the positional ordering peaks reflect the rectangular symmetry of the bacterial pattern, but the central spot is isotropic. This lack of orientational order in the FFT image is a result of the fact that the cells are oriented parallel to the angle of viewing, and when viewed along their long axis the rod-like cells lack orientational anisotropy. Moving across the substrate, as the posts get further apart, the positional ordering peaks get correspondingly closer together and the central spot becomes anisotropic as the cells lie in the plane of the substrate and normal to the viewing angle. Further across the pitch gradient, there is a point at which bacteria can bridge neighboring posts along the contracted [01] direction but can no longer do so along the stretched [10] direction of the array. Due to their contact area maximization behavior, the bacteria preferentially lie in the contracted direction, as can be seen by the vertical lines in the fluorescence image (figure 1(b)) and in the anisotropic stretching of the central spot in the same direction (figure 1(c)). This uniaxial orientational ordering confirms that the bacteria adopt specific and robust configurations when adhering to the substrate and demonstrates the influence of surface topography on bacterial assembly.

*3.1.2. Topographical features direct bacterial order and disorder.* By precisely controlling the topography of the post array, we further demonstrate the ability to drive long-range bacterial assembly from a disordered to an ordered state and vice versa. Starting with a HAR nanopost array that had been fabricated with a pitch gradient, we have fabricated a unique two-dimensional gradient substrate by adapting the structural transformation by electrodeposition of polymers (STEPS) technique [30], as shown in figure 2(a) and described in section 2.1. A gradient of nanopost diameters was thus superimposed in the orthogonal direction, creating a 2D combinatorial array as schematically shown in figure 2(b). Epoxy replicas of the combinatorial array were then fabricated using a double-casting soft lithography method [29]. *P. aeruginosa* cultures were grown to 18 h on the epoxy replicas, and the resulting attachment was studied along the pitch and diameter gradients of the substrate by fluorescence microscopy. Pronounced effects of both post pitch and diameter on the mode of bacterial attachment were observed.

For large-pitch regions of the array, increasing nanopost diameter drives the bacterial patterning to order, first in the [01] and [10] in-plane directions on the substrate, and with further increased diameter, the bacteria begin to orient normal to the substrate. This result recapitulates the effect of decreasing post pitch, showing that the wall-to-wall gap (pitch minus diameter), rather than the pitch or diameter *per se*, is the critical ordering parameter. The in-plane configuration is maximized with a gap of approximately $a_{10} = 0.90\ \mu$m. Correspondingly, the bacteria attaching on a region of the substrate with smaller pitch were observed

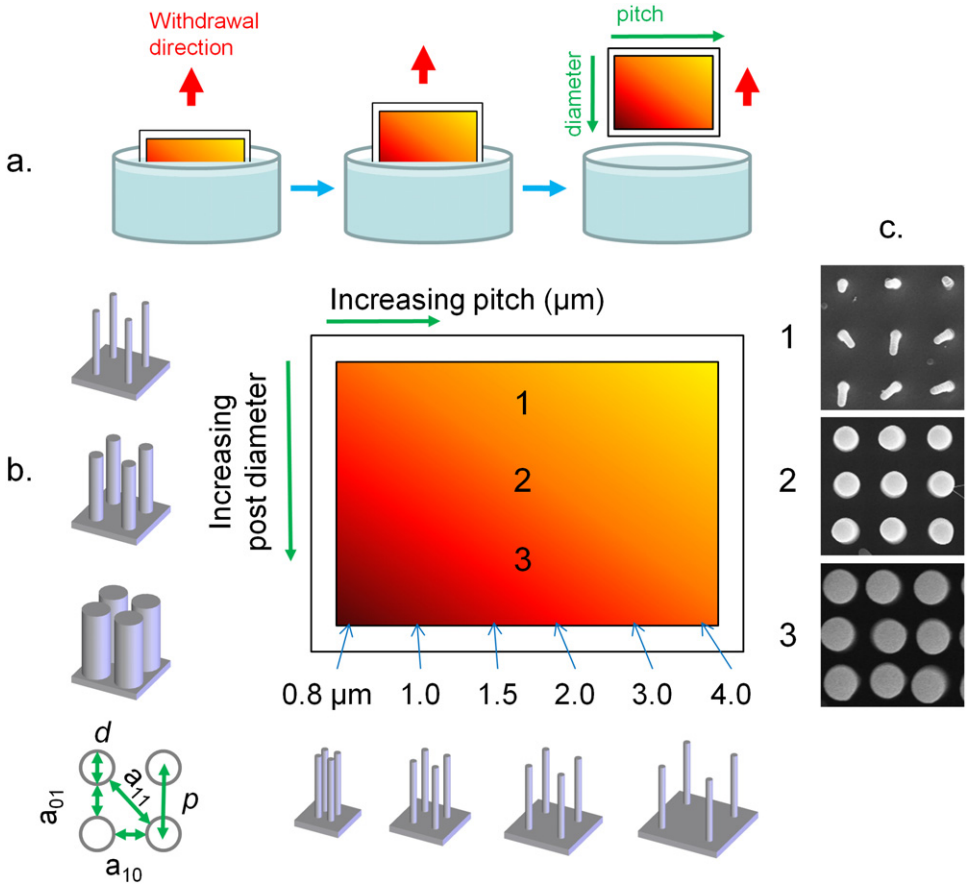


**Figure 2.** (a) Schematic of the orthogonal double-gradient substrate fabrication, adapting the recently described STEPS method [30]. A high-aspect-ratio nanopost array with a pitch gradient from left to right in the orientation shown above was withdrawn in discrete steps in the perpendicular direction from the electrodeposition bath, resulting in discrete increases in nanopost diameter from the top of the substrate to the bottom. This substrate was then replicated multiple times using a fast double-molding method [29]. (b) The final combinatorial substrate includes both a pitch ($p$) gradient from 0.8 to 4.0 $\mu$m and an orthogonal nanopost diameter ($d$) gradient from 300 nm to $\sim$1 $\mu$m. The interstitial spaces $a_{[10]}$ and $a_{[01]}$ are respectively the difference of $p - d$ in the [10] and [01] directions. (c) Top-down SEM images of the double-gradient nanoarray at three locations with $p = 1.66$ $\mu$m. The thin nanoposts at location 1 appear bent because they are flexible.

to first pattern in the [01], [10] arrangement, then assemble into the out-of-plane configuration with increasing diameter; diameter–pitch combinations producing a [11] gap dimension of about 1.05 $\mu$m maximize this configuration. Finally, the bacteria attachment becomes random and disordered as the spacing between posts further diminishes. At this point, the interstitial space is insufficient for the cells to insert between nearest-neighbor posts. Conversely, no orientational ordering results from combinations of pitch and native diameter in which the spacing is larger than the length of the bacterial cells, as expected from the contact area maximization behavior model [28]. The fluorescence microscopy images and corresponding FFTs in figures 3(a)–(c) demonstrate these finely controlled transitions between order-to-disorder, increasing order and disorder-to-order. Moreover, the length scale of the gap for optimal ordering closely correlates to the length scale of the bacterium, which is about 1 $\mu$m. Therefore, by designing a HAR nanostructured substrate with the appropriate length scale interstices, bacteria can be induced to order in arbitrary patterns.

### *3.2. Mechanical effects of nanostructured surfaces on biofilm growth*

In addition to controlling bacterial attachment to surfaces through the use of nanostructures and nanotopography, the mechanical properties of a surface have recently been reported to play a role [27]. This phenomenon was demonstrated using flat surfaces in the Young's modulus range of $\sim$1–$\sim$100 MPa and showed that there is a positive correlation between the density of attached bacteria and the substrate stiffness. The substrate stiffness in this case was modulated by the pH during fabrication of the polyelectrolyte multilayers. However, a bacteria-inhibitive material in the 1 MPa or lower stiffness regime may not be practical for some technological or device applications due to low mechanical rigidity. A monolithic material rather than a surface coating would also not be susceptible to potential delamination. In this study, we use HAR surface nanoarrays comprised of the bulk material to emulate a thin, ultra-compliant surface coating. The nanopost dimensions were 2 $\mu$m pitch, 250 nm diameter and 8 $\mu$m height. Bacteria near the nanoarray surface interact with highly flexible cantilevers rather than with a flat surface. The most

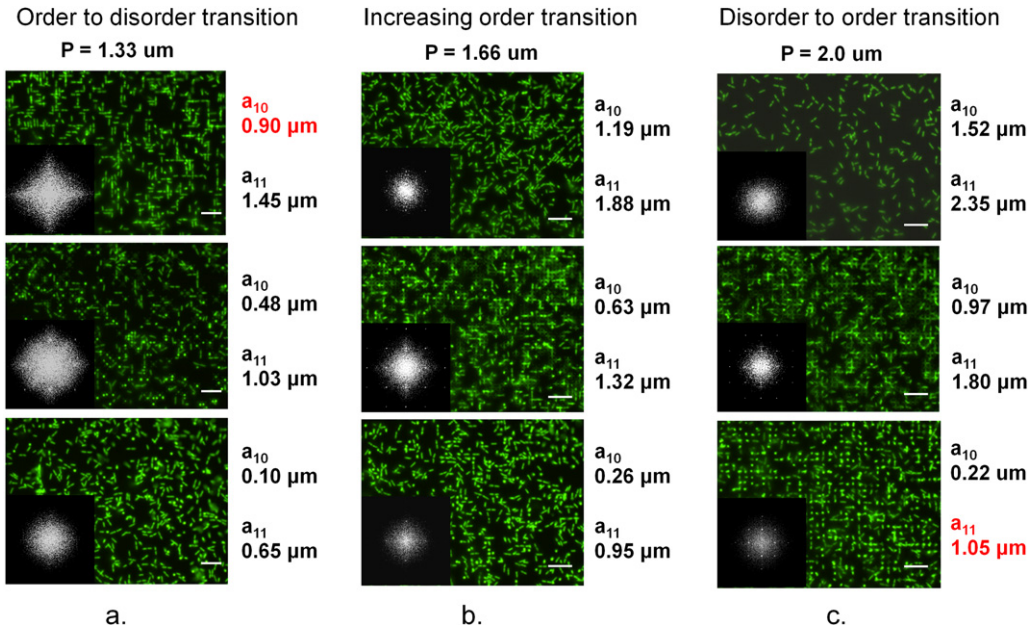


**Figure 3.** Fluorescence images and corresponding Fourier transforms of spontaneously patterned *P. aeruginosa* bacteria on the combinatorial nanoarray substrate. The image sequences show attachment along regions of equal pitch and increasing diameter, from top to bottom. The interstitial spacing, not center-to-center pitch, of the HAR nanoarray is the functional parameter of the substrate for spontaneous bacterial patterning on the surface. By precisely tuning nanoarray geometry, the effect can be controlled. $P$ is center-to-center [10] spacing; $a_{10}$ and $a_{11}$ are wall-to-wall [10] and [11] spacing. (a) An order-to-disorder transition is induced as the $a_{11}$ interstitial space is decreased to the point that bacteria can no longer insert between nearest-neighbor nanoposts. (b) Initially in-plane bacteria transition to out-of-plane order as the interstitial space becomes optimized for out-of-plane insertion. (c) Initially disordered bacteria transition to a high degree of order. Scale bars are 8 $\mu$m.

flexible nanoposts in our study deflect ∼5 $\mu$m/100 pN of force applied to the tip perpendicular to the long axis of the post, based on Eulerian beam mechanics: $\delta = \frac{Fl^3}{3EI}$, where $\delta$ is the tip deflection, $F$ applied force, $l$ post height, $E$ elastic modulus and $I$ moment of inertia. By comparison, for a bacterium to indent a flat surface ∼5 $\mu$m/100 pN, the elastic modulus would need to be ∼5 Pa. For this, we assume the 200 nm radius cells to apply force with their hemispherical poles and we use the Hertzian elastic contact model for indentation: $\delta = (\frac{4E}{3F(1-\nu^2)}R^{0.5})^{2/3}$, with $\delta$ the indentation depth, $\nu$ Poisson's ratio, $E$ elastic modulus, $F$ applied force and $R$ indenter radius. By this analysis, the soft, hair-like surface attains effective stiffnesses (force per unit deflection or deformation) six orders of magnitude lower than the constituent polymers, which are themselves in the range of 20–2000 MPa, seven to nine orders of magnitude higher Young's modulus than required for a flat surface.

*3.2.1. Cytophilicity screening of polymer surfaces.* Using the HAR nanoarray platform and a CFU biofilm quantification assay (see section 2), we investigated the attachment density of bacteria on surfaces as a function of the nanoarray effective stiffness. The effective stiffness was controlled by selection of the polymer so as to keep the nanoarray geometry constant. Candidate polymer systems were first screened for leaching toxicity to *P. aeruginosa*. Flat substrates made of each polymer were sputter-coated with 20 nm Au to mask their native surface chemistry and biofilms cultured on these substrates were quantified (figure S1 available at stacks.iop.org/Nano/22/494007/mmedia). The polyurethanes NOA65, 20 MPa; NOA61, 500 MPa; and the epoxy UVO-114, 2000 MPa were selected for their low leaching toxicity (as measured by high viable cell counts), photocurability and a broad range of modulus values. The relative cytophilicity of each of these three polymers without sputtering was similarly determined, showing slight differences in CFU, as shown in figure 4 (flat surfaces).

*3.2.2. Biofilm growth response to the effective stiffness of topographical features.* As seen in figures 4(a) and (b), the numbers of CFUs measured from 27 h biofilms cultured on 2 GPa and 500 MPa nanoarrays were larger than on the corresponding flat surfaces. This trend may be expected based on the nanoarrays' larger surface area versus flat substrates. However, a biofilm growth crossover regime occurs for the 20 MPa NOA65 polymer nanoarray. On this ultra-compliant structured surface, despite the surface area increase, resultant biofilm actually decreases with respect to the addition of HAR posts. Since the material cytophilicities are similar, these results suggest that the extremely low effective stiffness experienced by cells interacting with the soft, hair-like surface inhibits biofilm accumulation. (By comparison, *P. aeruginosa* forms indistinguishably robust biofilm after 24 h on a polymer surface, regardless of the surface chemical functionality, as seen in figure S2 (available at stacks.iop.org/Nano/22/494007/mmedia), suggesting its indifference to surface chemistry alone.) Based on the flexible cantilever model of nanoarray effective stiffness discussed above, the minimum threshold for

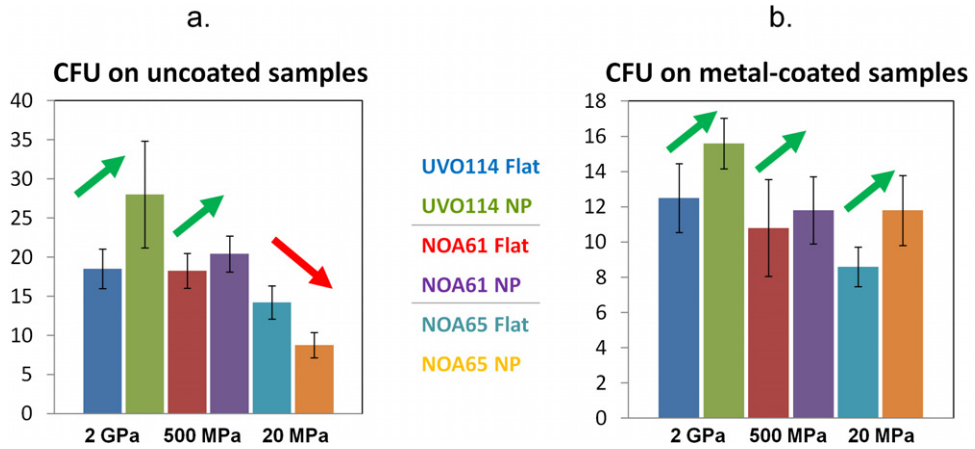


**Figure 4.** (a) Colony forming unit (CFU) measurements of *P. aeruginosa* biofilm growth on both unpatterned and high-aspect-ratio (HAR) nanopost substrates fabricated from polymers of varying Young's modulus. The UVO-114 (2 GPa) and NOA61 (500 MPa) nanopost substrates show increased growth versus the unpatterned control substrates. However, a biofilm growth crossover regime with respect to the addition of HAR nanoposts occurs in the softest polymer, NOA65. Despite a surface area increase, resultant biofilm decreases. (b) The crossover regime is not observed when a 20 nm gold coating is applied to the nanoposts, which increases their effective stiffness, indicating the upper bound of an effective stiffness range for biofilm growth inhibition. CFU were based on $10^{-4}$ dilutions.

this mechanoselective behavior is of the order of 5 $\mu$m surface deformation per 100 pN force—equivalent to a bacterium attaching to a flat surface with an elastic modulus of ∼5 Pa.

In contrast, the growth crossover regime is not observed once a 20 nm gold layer is applied to the same three polymer nanoarrays, as shown in figure 4(b). The estimated effect of the gold layer, whose modulus is 79 GPa, is to stiffen by about 20× the polymer–metal core–shell nanoposts. With this increase in the HAR nanoarray effective stiffness, the growth crossover in the 20 MPa polymer nanoarray is not observed, suggesting the upper bound of a biofilm growth inhibition range. These effective stiffness values are themselves lower estimates, as bacteria are in contact with not only the distal ends of the nanoposts, but also the geometrically stiffer basal ends, and indeed with the basal plane. The 'average' effective stiffness of these surfaces, at which the mechanoselective adhesion phenomenon occurs, can be assumed to be higher.

Regardless, the passively dynamic nature of such surfaces may present an unstable and unfavorable attachment target for bacteria. Their deformation under imposed bacterial forces can cause them to read as a fluid-like solid, whereas biofilms seek secure and immobile surfaces to colonize. Therefore, the principle of effective stiffness-mediated inhibition of bacterial attachment may constitute promising surface treatments in diverse applications for preventing biofilm accumulation.

## 4. Conclusions

By applying a novel combinatorial platform, we have elucidated key nanometer-scale geometric and mechanical parameters of surfaces that drive long-range bacterial adhesion patterns and biofilm growth behavior. The interstitial spacing between surface features is experimentally confirmed to be the critical parameter controlling assembly and it can be used to induce specific ordering phases using a range of feature sizes of the order of the bacterial cell. Furthermore, for the first time, the mechanoselective attachment of bacteria on compliant high-aspect-ratio nanostructures has been described. This extends the recent finding of bacterial mechanosensitivity to a much lower effective stiffness regime of ∼50 $\mu$m nN$^{-1}$, equivalent to flat films with a modulus as low as 5 Pa. Moreover, it suggests a completely new strategy to exploit mechanoselective adhesion. When the effective compliance of the hair-like nanoarray is increased beyond a threshold, biofilm growth is inhibited as compared to a flat control surface. As this is strictly a mechanical–structural property and does not rely on surface chemical functionalization, it is not susceptible to masking and may be persistent. As a potential new strategy, HAR nanoarrays mimicking an extremely compliant flat surface offer promise for diverse applications for controlling and inhibiting biofilm accumulation.

## Acknowledgments

We thank Dr. Yunrong (Win) Chai, Dr. Sigolene Lecuyer and Anna Wang for the biological techniques. The work was supported by the Office of Naval Research (Award No. N000141110641) and BASF Advanced Research Initiative at Harvard University.

## References

[1] Shapiro J 1998 Thinking about bacterial populations as multicellular organisms *Annu. Rev. Microbiol.* **52** 81–104
[2] Costerton J W and Stewart P S 2001 Battling biofilms—the war is against bacterial colonies that cause some of the most tenacious infections known. The weapon is knowledge of the enemy's communication system *Sci. Am.* **285** 74–81
[3] Christie A O and Dalley R 1987 Barnacle fouling and its prevention *Barnacle Biology* ed A J Southward (Rotterdam: CRC/Balkema) pp 419–33
[4] Davies D 2003 Understanding biofilm resistance to antibacterial agents *Nature Rev. Drug Discov.* **2** 114–22

[5] Klevens R *et al* 2007 Estimating health care-associated infections and deaths in US hospitals, 2002 *Public Health Rep.* **122** 160–6
[6] Marsh P 2005 Dental plaque: biological significance of a biofilm and community life style *J. Clin. Periodontol.* **32** 7–15
[7] Blango M and Mulvey M 2009 Bacterial landlines: contact-dependent signaling in bacterial populations *Curr. Opin. Microbiol.* **12** 177–81
[8] Ben-Jacob E, Cohen I and Gutnick D L 1998 Cooperative organization of bacterial colonies: from genotype to morphotype *Ann. Rev. Microbiol.* **52** 779–806
[9] Klausen M *et al* 2003 Involvement of bacterial migration in the development of complex multicellular structures in Pseudomonas aeruginosa biofilms *Mol. Microbiol.* **50** 61–8
[10] Stewart P S and Franklin M J 2008 Physiological heterogeneity in biofilms *Nature Rev. Microbiol.* **6** 199–210
[11] Vlamakis H *et al* 2008 Control of cell fate by the formation of an architecturally complex bacterial community *Genes Dev.* **22** 945
[12] Epstein A *et al* 2010 Bacterial biofilm shows persistent resistance to liquid wetting and gas penetration *Proc. Natl Acad. Sci.* **108** 995–1000
[13] Banerjee I, Pangule R and Kane R 2010 Antifouling coatings: recent developments in the design of surfaces that prevent fouling by proteins, bacteria, and marine organisms *Adv. Mater.* **23** 690–718
[14] Park K D *et al* 1998 Bacterial adhesion on PEG modified polyurethane surfaces *Biomaterials* **19** 851–9
[15] Prime K L and Whitesides G M 1991 Self-assembled organic monolayers: model systems for studying adsorption of proteins at surfaces *Science* **252** 1164
[16] Bos R *et al* 2000 Retention of bacteria on a substratum surface with micro patterned hydrophobicity *FEMS Microbiol. Lett.* **189** 311–5
[17] Gristina A 1987 Biomaterial-centered infection: microbial adhesion versus tissue integration *Science* **237** 1588
[18] Neu T 1996 Significance of bacterial surface-active compounds in interaction of bacteria with interfaces *Microbiol. Rev.* **60** 151–66
[19] Hall-Stoodley L, Costerton J W and Stoodley P 2004 Bacterial biofilms: from the natural environment to infectious diseases *Nature Rev. Microbiol.* **2** 95–108
[20] Trevors J 1987 Silver resistance and accumulation in bacteria *Enzyme Microbial Technol.* **9** 331–3
[21] Costerton J, Stewart P and Greenberg E 1999 Bacterial biofilms: a common cause of persistent infections *Science* **284** 1318
[22] Schumacher J *et al* 2007 Engineered antifouling microtopographies—effect of feature size, geometry, and roughness on settlement of zoospores of the green alga Ulva *Biofouling* **23** 55–62
[23] Discher D, Janmey P and Wang Y 2005 Tissue cells feel and respond to the stiffness of their substrate *Science* **310** 1139
[24] Huebsch N *et al* 2010 Harnessing traction-mediated manipulation of the cell/matrix interface to control stem-cell fate *Nature Mater.* **9** 518–26
[25] Stevens M M and George J H 2005 Exploring and engineering the cell surface interface *Science* **310** 1135–8
[26] Davey M and O'toole G 2000 Microbial biofilms: from ecology to molecular genetics *Microbiol. Mol. Biol. Rev.* **64** 847
[27] Lichter J *et al* 2008 Substrata mechanical stiffness can regulate adhesion of viable bacteria *Biomacromolecules* **9** 1571–8
[28] Hochbaum A and Aizenberg J 2010 Bacteria pattern spontaneously on periodic nanostructure arrays *Nano Lett.* **10** 3717–21
[29] Pokroy B *et al* 2009 Fabrication of bioinspired actuated nanostructures with arbitrary geometry and stiffness *Adv. Mater.* **21** 463–9
[30] Kim P *et al* 2011 Structural transformation by electrodeposition on patterned substrates (STEPS): a new versatile nanofabrication method *Nano Lett.* doi:10.1021/nl200426g